

Luminosity Distribution of Dwarf Elliptical-like Galaxies

Mira Seo,¹[★] Hong Bae Ann,¹

¹*Department of Earth Sciences, Pusan National University, 46241, Busan, Korea*

Accepted 2022 June 10. Received 2022 May 29; in original form 2021 October 2

ABSTRACT

We present the structural parameters of ~ 910 dwarf elliptical-like galaxies in the local universe ($z \lesssim 0.01$) derived from the r -band images of the Sloan Digital Sky Survey (SDSS). We examine the dependence of structural parameters on the morphological types (dS0, dE, dE_{bc}, dSph, and dE_{blue}). There is a significant difference in the structural parameters among the five sub-types if we properly treat the light excess due to nucleation in dSph and dE galaxies. The mean surface brightness within the effective radius ($\langle \mu_e \rangle$) of dSph galaxies is also clearly different from that of other sub-types. The frequency of disk features such as spiral arms depends on the morphology of dwarf galaxies. The most pronounced difference between dSph galaxies and other sub-types of early-type dwarf galaxies is the absence of disk feature which is thought to be closely related to their origin.

Key words: galaxies: general – morphology – dwarf – environment

1 INTRODUCTION

Dwarf galaxies are most abundant in the local universe and they are supposed to be building blocks of massive galaxies in the Λ CDM cosmology (Boselli & Gavazzi 2014). Dwarf galaxies can be divided into two groups. One is the dwarf elliptical-like galaxies (hereafter dE-like galaxies) of which basic morphology resembles the dwarf elliptical galaxy (dE) and the other is the dwarf irregular galaxy (dI). Ann, Seo & Ha (2015, hereafter ANN15) classified the dE-like galaxies by five subtypes, dS0, dE, dE_{bc}, dSph, and dE_{blue} using colour images of the Sloan Digital Sky Survey (SDSS). The dS0 is dwarf lenticular galaxy introduced by Sandage & Binggeli (1984) and the subtypes dE_{bc} and dE_{blue} represents dE galaxies with blue core and globally blue dwarfs with ellipsoidal shape, respectively. In the traditional photographic plates, dE_{bc} and dE_{blue} could not be distinguished from dE. In the literature, dSph galaxies are not always distinguished from dE galaxies (Sandage & Binggeli 1984; Ferguson & Binggeli 1994; Kormendy & Bender 2012). However, many studies treated the dSph galaxy as a distinct class of galaxy (Mateo 1998; Gallagher & Wyse 1994; Grebel 1997; van den Bergh 1999). Among the five sub-types of dE-like galaxies, dS0, dE and dSph are considered to be early-type dwarfs while dE_{blue} galaxies are taken as late-type galaxies if we group them by the presence of on-going star formation. The subtype dE_{bc} is intermediate between them because of the active star formation in the core only. We considered dE_{bc} galaxies as early-type dwarfs because their global photometric properties are similar to dS0, dE and dSph galaxies (Ann 2017).

The dE-like galaxies have surface brightness distribution different from the giant elliptical galaxies which are well described by

the $r^{1/4}$ -law. The surface brightness profile of dE-like galaxies, dE in particular, is best fitted with Sérsic index n less than 2 (Binggeli & Jerjen 1998; Ryden et al. 1999; Grant et al. 2005; Kim et al. 2006; Janz et al. 2014). Moreover, a significant fraction of dE-like galaxies show disk features which have a variety of structures such as spiral arms and bars (Jerjen et al. 2000; Barazza et al. 2002; Geha et al. 2003; Graham et al. 2003; De Rijcke et al. 2003; Lisker et al. 2006). Most disk features can be seen from the residual images made by subtracting axisymmetric component or from the unsharp masked images. Some of the spiral arms are grand-design arms which are mostly observed in early-type spiral galaxies (Elmegreen & Elmegreen 1982; Ann & Lee 2013).

Presence of disk structures such as spiral arms and bars in dE galaxies raises doubts on the conventional belief that they are primordial object collapsed in the early epoch of galaxy formation and suggests a different channel to their formation at least for dE galaxies with disk features. The most popular scenario for the origin of the early-type dwarf galaxies with disk features is that they are transformed objects from the late-type galaxies of which their cold gas was removed by the ram pressure from the hot intracluster medium (Gunn & Gott 1972). In addition, the structure of a galaxy can be modified by the tidal field of the group and cluster when they enter into them (Moore et al. 1998, 1999). The rapid rotation observed in some dwarf elliptical galaxies supports the hypothesis that the dwarf elliptical galaxies are transformed from the spiral galaxies by losing their gas in groups and clusters. Since the majority of dE-like galaxies are members of groups or clusters (Ann 2017), the environmental quenching (Peng et al. 2010), a sudden shutdown of star formation, caused by ram pressure stripping (Gunn & Gott 1972) together with galaxy harassment (Moore et al. 1998, 1999) and tidal shock (Mayer et al. 2001) can transform late-type galaxies into early-type dwarfs.

[★] E-mail: mrseo@pusan.ac.kr

It seems of interest to see whether the structural parameters and the embedded disk features of dE-like galaxies are distinguished for the five sub-types. In particular, we are very interested to see whether the structural difference between dE and dSph is significant enough to reflect their morphological difference. In general, dE-like galaxies with $M_B < -14$ are considered as dwarf elliptical galaxies while those fainter than $M_B = -14$ are considered as dwarf spheroidal galaxies. However, there are some overlaps in their luminosity distribution (ANN15). Moreover, the morphological difference between dE and dSph is based on the differences in surface brightness and its gradient (ANN15). The dSph galaxies show faint surface brightness with shallow gradient than the dE galaxies. In addition, there is pronounced differences in the dynamical property and dark matter content. The dE galaxies are supposed to be supported by the rapid rotation while the dSph galaxies are supported by the velocity dispersion (Geha et al. 2002, 2003; Koch et al. 2007). However, it does not mean that all dSph galaxies have no rotation and all dE galaxies are fast rotators. Rather, some dSph galaxies have significant rotations (del Pino et al. 2017) and some dE galaxies are slow rotators (Toloba et al. 2015). The dSph galaxies have much larger fraction of dark matter than the dE galaxies (Mateo 1998; Gilmore et al. 2007).

To examine the structural differences among dE-like galaxies, we analysed their luminosity distributions using the GALFIT (Peng et al. 2002) which is known to be effective to analyse the two-dimensional luminosity distribution of galaxies. We examined the residual images obtained by subtracting the GALFIT model images from the observations to see the disk features. Since the majority of dS0, dE, and dSph galaxies have nuclear component (ANN15), we apply multi-component models to dS0, dE, dSph galaxies along with dE_{bc} galaxies. The main purpose of the present study is to derive the Sérsic index of the main component to know their statistics. We also examine whether the sub-types of the dE-like galaxies have significantly different structures.

The present paper is organized as follows. In section II, we describe the data and method. The results are presented in section III. Discussion is presented in section IV and a brief summary and conclusions are given in the last section.

2 DATA AND METHOD

2.1 Data selection

Our galaxy sample is ~910 dE-like galaxies divided into 5 sub-types (dS0, dE, dSph, dE_{bc}, dE_{blue}) from the galaxy catalogue of ANN15. It is a visually classified galaxy catalogue of the local universe with $z \lesssim 0.01$ using SDSS DR7. Our dE-like galaxy sample is a part of the 5,386 galaxies of ANN15. Some sample galaxies are presented in Figure 1.

Data of ANN15 is basically taken from KIAS-VAGC (Choi et al. 2010) and some faint galaxies are added from the NED(NASA Extragalactic Data) and Makarov & Karachentsev (2011) catalogues. KIAS-VAGC is based on the New York University Value-added catalogue(NYU-VAGC; Abazajian et al. (2009)) using SDSS DR7 and contains several physical quantities of galaxies including the computer-based automatic classification (Park & Choi 2005). Makarov & Karachentsev (2011) catalogue is a list of galaxy group in the local universe with $|b| > 15^\circ$ and with $V_{LG} < 3,500 \text{ km s}^{-1}$ for a local Group, and have classifications of 10,914 galaxies based on the RC3 classification.

We used the galaxy distances given by ANN15 who calculated

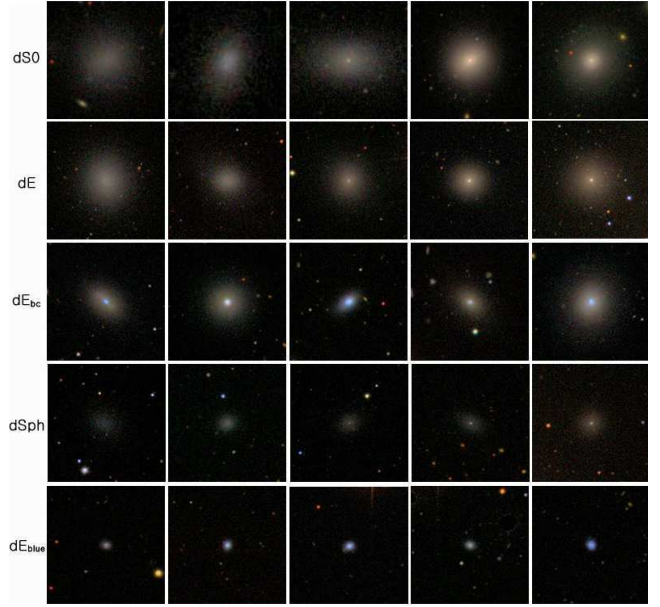


Figure 1. Sample images for dwarf elliptical-like galaxies: dS0 (first row), dE (second row), dE_{bc} (third row), dSph (fourth row) and dE_{blue} (fifth row). Left two columns are non-nucleated galaxies and right three columns are nucleated galaxies in dS0, dE, dSph galaxies. (It is made by the images in Figure 5 of ANN15).

the distances of galaxies using the V_{LG} obtained from the observed redshift by the method of Mould et al. (2000) assuming the Hubble constant $H = 75 \text{ km s}^{-1} \text{ Mpc}^{-1}$. For the galaxies in the Virgo Cluster, the distance of the Virgo Cluster was applied. On the other hand, for galaxies of which the metric distances are given in the NED, the metric distances were used.

2.2 Method

We use r-band images of SDSS (York et al. 2000; Stoughton et al. 2002) Data Release 7 (Abazajian et al. 2009) for GALFIT (Peng et al. 2002, 2010). We first constructed a single-component model with a Sérsic function which is known to represent the surface brightness distribution of dE-like galaxies. In the case of dS0 galaxies, which are early-type dwarf galaxies containing disk component (Binggeli et al. 1985), so we have applied two-components model with a Sérsic + exponential disk functions. And the basic parameters like integrated magnitude, effective radius, axis ratio and position angle, required for GALFIT model are taken from the SDSS casjob. However, applying a single component model to nucleated dE, dS0 and dSph galaxies, there is an excess of light in the central region of the residual image, which appears as a ring, oval, or disk in the central regions of galaxies.

To treat the excess of light in the central regions of galaxies, we add a nuclear component to single Sérsic function. There are two useful functions in GALFIT for fitting the luminosity of the nuclear region of dwarf galaxy, the empirical (modified) King profile(Elson 1999) and the Nuker profile(Lauer et al. 1995). We apply these functions to analyse the luminosity of our sample. Thus, we have modelled the nucleated dE-like galaxies of dE_n, dSph_n, and dE_{bc} with the Sérsic profile + King/Nuker profile, and non-nucleated galaxies of dE_{un}, dSph_{un}, and dE_{blue} with the Sérsic profile. And for dS0 galaxies, we used three and two components models including

Table 1. Fitting models of dE-like galaxies for GALFIT

<i>type</i>	Functions
dS0 _n	Sérsic + expDisk + King/Nuker
dS0 _{un}	Sérsic + expDisk
dE _n	Sérsic + King/Nuker
dE _{un}	Sérsic
dSph _n	Sérsic + King/Nuker
dSph _{un}	Sérsic
dE _{bc}	Sérsic + King/Nuker
dE _{blue}	Sérsic

exponential disk profile for dS0_n and dS0_{un} galaxies, respectively (see Table 1).

3 RESULTS

We examined the structural parameters derived from the GALFIT along with the luminosity (M_r) derived from the model r -magnitude corrected for the extinction caused by the dust in the Galaxy. We described the Sérsic index (n) separately but other parameters such as R_e and $\langle\mu_e\rangle$ are examined in the correlation analysis only. Here, R_e is the effective radius within which half of the galaxy's luminosity is contained and $\langle\mu_e\rangle$ is the mean surface brightness within R_e .

3.1 Luminosity of dE-like galaxies

Dwarf galaxies are known to have luminosity fainter than $M_B \approx -18$. Figure 2 shows the luminosity distributions of the three sub-types (dS0, dE, and dSph) of dE-like galaxies, compared with that of the dE-like galaxies in the EVCC (Kim et al. 2014). We use a distance of 16.65 Mpc for the Virgo cluster to convert the SDSS r -band model magnitudes of sample galaxies to the absolute magnitudes M_r . The top panel presents the luminosity distribution of the EVCC sample. The total sample is plotted as gray-coloured region, and red and orange lines represent the distributions of dEs (red) and dS0s (orange), respectively. The middle and bottom panels show the luminosity distribution of our sample; dS0s and dEs in the middle panel and dS0s, dEs, and dSphs in the bottom panel. The green line in the bottom panel represent dSph galaxies in our sample.

At a glance, there seems to be a large difference between the luminosity distributions of dE and dS0 galaxies in the two samples. There are a lot of faint dE galaxies ($M_r > -15$) in the EVCC while only a small fraction of faint dE galaxies in our sample. It is due to the inclusion of dSph galaxies in the dE sample of the EVCC, whereas we separate dSph galaxies from the dE sample. Almost all dSph galaxies in our sample are classified as dE in the EVCC. As shown in the bottom panel of Figure 2, the luminosity distribution of dSph galaxies is much different from those of dE and dS0 galaxies. The fraction of dSph galaxies that are fainter than $M_r = -15$ is about three times larger than that of dSph galaxies that are brighter than $M_r = -15$. Our sample has more fainter dE-like galaxies than the EVCC sample because our sample includes local dwarf galaxies whose distances are closer than the Virgo cluster.

If we compare the luminosity distributions of dwarf galaxies without sub-type division, which are plotted as grey regions in the top and bottom panels, there is not much difference except for the peak luminosity. The difference in the luminosity distributions of the EVCC dwarfs (top panel) and our sample (bottom panel) is

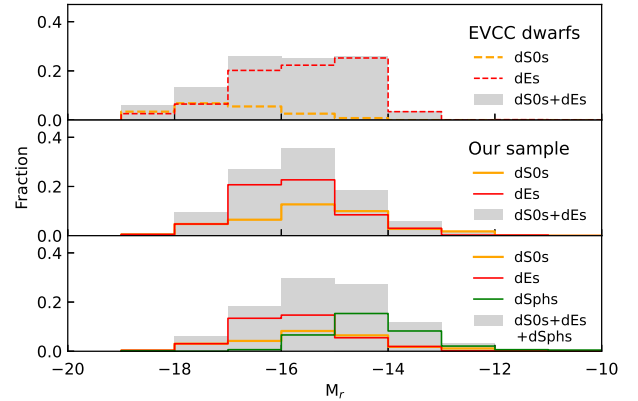


Figure 2. Luminosity distributions of early type dwarf galaxies of our sample and EVCC. Top panel is dE+dS0 galaxies of the EVCC. Middle panel shows dS0s+dEs of our sample and bottom panel presents dEs+dS0s+dSphs of our sample. The grey shaded regions show the sum of sub-types. Red lines represents dE galaxies, orange lines for dS0s and green lines for dSphs, respectively.

due to the difference in the mean distance of the two samples. Our sample consists of all the early-type dwarfs (dS0 + dE + dSph) with redshift less than $z = 0.01$ observed in the SDSS while the EVCC sample consists of dwarfs in the Virgo cluster only. Thus, our sample includes more fainter dwarfs than the EVCC sample. However, it is also affected by the different environment of the two samples. The higher fraction of fainter galaxies ($M_r > -14$) in our sample is due to the galaxies closer than the Virgo cluster whereas the higher fraction of brighter galaxies ($M_r < -16$) in the EVCC is thought to be caused by the environmental effect since the high galaxy density of the Virgo cluster is favorable for luminous dwarfs if the luminosity-density relation observed for giant galaxies (e.g., Park et al. 2007) holds for dwarf galaxies.

Another point worth to be noted is that the luminosity distributions of dE and dS0 galaxies are quite similar in our sample (middle panel) while those of EVCC sample are very different. The highest fraction of dS0 in our sample occurs at $M_r = -15.5$ while that of EVCC sample occurs at $M_r = -17.5$, two magnitudes brighter. It seems to be due to classification criteria for dS0 galaxies applied by ANN15 who considered a dE-like galaxy with a central lens-like component as a dS0 galaxy while dS0 in the EVCC sample has a lens or small bulge. We think some of the brightest dS0 in the EVCC sample are S0 galaxies in ANN15 as suggested by their luminosity.

3.2 Sérsic index of dE-like galaxies

We conducted a two-dimensional image decomposition using the r -band images of dE-like galaxies by applying the GALFIT (Peng et al. 2002) in order to analyse their photometric properties. GALFIT assumes the Sérsic function as the basic luminosity profiles of galaxies together with several other functions such as King profile (Elson 1999) and Nuker profile (Lauer et al. 1995). The Sérsic profile is expressed as

$$\mu(R) = \mu_e + 1.086b_n \left[\left(\frac{R}{R_e} \right)^{1/n} - 1 \right]$$

where μ_e is effective surface brightness at R_e , n is the Sérsic index, and b_n is coupled to n to ensure that half of the total flux is always within R_e .

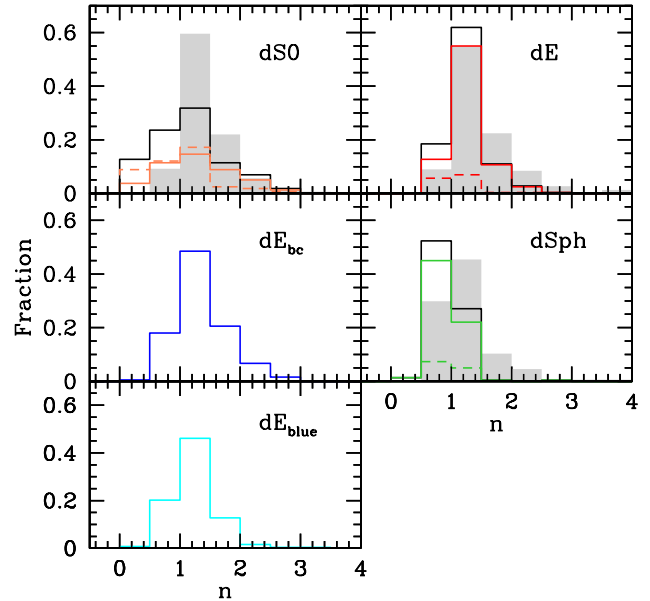
Table 2. Fraction of Sérsic Index (n) of dE-like galaxies.

n	dS0	dS0 _{un}	dS0 _n	dE	dE _{un}	dE _n	dSph	dSph _{un}	dSph _n	dE _{bc}	dE _{blue}
0 ~ 0.5	0.13	0.09	0.04	0.00	0.00	0.00	0.01	0.00	0.01	0.01	0.01
0.5 ~ 1.0	0.24	0.12	0.11	0.18	0.06	0.13	0.52	0.07	0.45	0.18	0.20
1.0 ~ 1.5	0.32	0.17	0.15	0.62	0.07	0.55	0.27	0.05	0.22	0.48	0.46
1.5 ~ 2.0	0.11	0.03	0.09	0.11	0.00	0.11	0.00	0.00	0.00	0.21	0.13
2.0 ~ 2.5	0.07	0.02	0.05	0.03	0.00	0.02	0.00	0.00	0.00	0.07	0.02
2.5 ~ 3.0	0.02	0.01	0.01	0.00	0.00	0.00	0.00	0.00	0.00	0.02	0.00
3.5 ~ 4.0	0.00	0.00	0.00	0.00	0.00	0.00	0.00	0.00	0.00	0.00	0.00

Figure 3 shows the distributions of the Sérsic index (n) derived for the five sub-types of dE-like galaxies. For dS0, dE, and dSph galaxies, the distributions of Sérsic index n are further divided into the galaxies with and without nucleation. We present the total distributions by black solid lines and the galaxies with and without nucleation by colored solid and dashed lines, respectively. In cases of dE_{bc} and dE_{blue} galaxies, only the total distributions are plotted. The dE_{bc} galaxies are considered to have no nuclei but cores and the dE_{blue} galaxies have no nuclei. The Sérsic index n presented in Figure 3 is the Sérsic index fitted to the main component of each galaxy. In cases of nucleated dS0, dE, and dSph galaxies which are denoted as dS0_n, dE_n, and dSph_n, respectively in the catalogue of ANN15 and dE_{bc} galaxies that have blue cores, we used two or three component models in GALFIT. One is the Sérsic profile and the other is either King profile or Nuker profile. For dS0 galaxies, exponential disk profile is added to other models. We considered the King profile preferentially as the luminosity distribution of a nucleation, but we used the Nuker profile when the King profile fails to approximate the nuclear luminosity. We summarize the fitting models in Table 1.

The Sérsic index n , as shown in Figure 3, is in the range of 0.5 to 3.0 with some differences among sub-types. When we apply a single component model (shaded region), the dS0 and dE galaxies show similar distributions. But, they are quite different if we use Sérsic + exponential disk + nuclear component in dS0s and Sérsic + nuclear component in dEs. The dS0 galaxies have n mainly in the range of 0.5~2.0, while dE galaxies have n in the range of 1.0~2.0. The dE_{bc} galaxies have similar ranges as the dE galaxies, but have more fractions in larger n . The Sérsic index n of dSph and dE_{blue} galaxies are mostly in the range between 0.5 and 1.5. As shown in Table 2, more than 50% of dE galaxies have n between 1.0 and 1.5. The most frequent n in dS0s is similar to that of dEs, but the distributions of n are not similar. More than 50% of dEs have n between 1.0~1.5, while less than 40% of dS0s have n in the same range. The distribution of n in dS0s is wider than that in dEs, and the fractional frequency is slightly decreased toward small n in dS0s. The dSph galaxies have a different distribution from dS0 and dE galaxies. The maximum frequency of n is shifted to a smaller value, and the width of the distribution is narrow. In other words, galaxies with $n = 0.5 \sim 1.0$ are most abundant, followed by galaxies with $n = 1.0 \sim 1.5$.

We applied the Kolmogorov-Smirnov (K-S) test to examine the statistical significance of the differences in the frequency distributions of the Sérsic index n among the five sub-types of dE-like galaxies. We summarize the result of K-S test in Table 3 where D_{K-S} is K-S statistic representing the maximum difference in the cumulative distributions of two samples and p is the p -value corresponding to D_{K-S} . We used the K-S statistic D_α with a significance level of $\alpha = 0.05$ to test the null hypothesis that the two samples

**Figure 3.** Frequency distributions of the Sérsic index of dE-like galaxies. The total distribution is represented by black solid line and galaxies with and without nucleation are coloured solid and dashed lines, respectively. Shaded regions designate the Sérsic index derived from single component models.

are drawn from the same population. We rejected the null hypothesis if $D_{K-S} \geq D_\alpha$ or p -value less than α . As can be inferred from the p -values in Table 3, each sub-type of dE-like galaxies has Sérsic index statistically different from those of other sub-types except for similar Sérsic index for dE and dE_{blue} galaxies. However, there is no significant distinction between the nucleated dwarfs and non-nucleated dwarfs except for dSph galaxies.

3.3 Correlations between structural parameters

We examine the correlations between the structural parameters derived from GALFIT (n , R_e , $\langle \mu_e \rangle$, b/a) together with M_r . Here $\langle \mu_e \rangle$ is the mean surface brightness within R_e . We present some examples in Figure 4. We use colour coded symbols for easy distinction of the sub-types: dS0(orange), dE(red), dE_{bc}(blue), dSph(green), and dE_{blue}(cyan). There are fairly good correlations among the three parameters, M_r , R_e , and $\langle \mu_e \rangle$ if we consider all the sub-types as a whole, whereas axial ratio (b/a) shows little or no correlations with other parameters. In case of the Sérsic index n , it shows a weak correlation with $\langle \mu_e \rangle$ if we consider all the sub-types except dS0. What is remarkable is that the sub-types of dE-like galaxies are fairly well distinguished in the diagrams for parameters

Table 3. K-S test of Sérsic Index (n) for five sub-types of dE-like galaxies.

types	D_{K-S}	p	sample size
dS0, dE	0.2781	< 0.0001	140, 231
dS0, dE _{bc}	0.2623	< 0.0001	140, 186
dS0, dSph	0.3606	< 0.0001	140, 179
dS0, dE _{blue}	0.2559	< 0.0001	140, 229
dE, dE _{bc}	0.1698	0.0053	231, 186
dE, dSph	0.4720	< 0.0001	231, 179
dE, dE _{blue}	0.0894	0.3172	231, 229
dE _{bc} , dSph	0.5289	< 0.0001	186, 179
dE _{bc} , dE _{blue}	0.1960	0.0008	186, 229
dSph, dE _{blue}	0.3958	< 0.0001	179, 229
dS0 _n , dS0 _{un}	0.2271	0.0542	72, 68
dE _n , dE _{un}	0.4293	0.0001	198, 33
dSph _n , dSph _{un}	0.1898	0.3806	152, 27

M_r , R_e , and $\langle \mu_e \rangle$ except for the indistinguishable two sub-types. dE and dS0, which have similar structural parameters with $M_r = -15.73 \pm 1.11$, $\log(R_e) = -0.09 \pm 0.28$, $\langle \mu_e \rangle = 22.86 \pm 0.97$ for dE galaxies and $M_r = -15.37 \pm 1.54$, $\log(R_e) = -0.19 \pm 0.36$, $\langle \mu_e \rangle = 22.41 \pm 1.66$ for dS0 galaxies, respectively. The reason for the similarity in the structural parameters of dS0 and dE galaxies is their similar origin, transformed from the late-type galaxies.

Among the correlations between structural parameters of dE-like galaxies, the correlation between $\langle \mu_e \rangle$ and M_r presented in the bottom left panel of Figure 4 is of a special interest because it plays a key role to distinguish dwarf ellipticals from giant ellipticals. Kormendy (1985) showed that the correlation between $\langle \mu_e \rangle$ and M_r for dwarf elliptical galaxies shows a trend opposite to the correlation observed for giant elliptical galaxies. There is a count argument that the two relations are continuous (Graham et al. 2003). Detailed analysis of the correlation between $\langle \mu_e \rangle$ and M_r were given by Kormendy & Bender (2012) which supports the opposite behaviour raised by Kormendy (1985). It dictates the increasing luminosity with increasing surface brightness for dwarf elliptical galaxies and an opposite trend for giant elliptical galaxies.

As shown in Figure 4, most correlations show weak or moderate correlations with the strongest one for the correlation between M_r and $\log(R_e)$ which has the Pearson correlation coefficient (cc) of -0.58. However, if we examine the correlation between M_r and $\log(R_e)$ for each sub-type of dE-like galaxies, the correlation strengths become higher with the strongest correlation for dSph galaxies that have cc = -0.71 and the weakest correlation for dE_{bc} galaxies that have cc = -0.59. The dS0, dE and dE_{blue} galaxies have similar correlation strength as cc = -0.63, -0.67, and -0.65, respectively. The slope, i.e., regression coefficient, of the relation between M_r and $\log(R_e)$ for dSph galaxies is -3.18 ± 0.23 with confidence interval of (-4.53, -1.85) and the slopes of other sub-types are within the confidence interval for dSph which is derived from the 1000 bootstrap resampling. The strongest correlation observed for the structural parameters M_r and R_e seems to reflect the well established relationship between the luminosity and size of galaxies (Blanton 2003; Shen et al. 2003).

It is clear that the luminosity of dSph galaxies is similar to dE_{blue} galaxies but they have completely different surface brightness. On average, the surface brightness of dSph galaxies is lower than other sub-types of dE-like galaxies whereas that of dE_{blue} galaxies is higher than other sub-types except for dE_{bc} galaxies of which surface brightness is similar to dE_{blue} galaxies. The high surface brightness of dE_{blue} galaxies is due to their small size. Since

dSph galaxies share structural properties with dS0, dE, and dE_{bc} galaxies except for $\langle \mu_e \rangle$, they do not share structural properties with dE_{blue} galaxies except for the luminosity and axis ratio (b/a). It seems likely that formation and evolution of dSph and dE_{blue} galaxies are much different. On the other hand, dS0 galaxies are difficult to distinguish from other sub-types of galaxies because bright part of these galaxies ($M_r < -15$) are almost indistinguishable in surface brightness and luminosity from dE galaxies, and faint part lies in the regions where dE_{blue} galaxies are likely to be located. The dE_{bc} galaxies are located everywhere except for the regions with $M_r > -13$. The dE galaxies, which are a typical type of dE-like galaxies, are distinct from dSph or dE_{blue} galaxies, but they have structural parameters similar to dS0 and dE_{bc} galaxies.

As shown in the bottom right panel of Figure 4 there is a moderate correlation between $\langle \mu_e \rangle$ and $\log(R_e)$ of dE-like galaxies with cc = 0.46. The effective radii decrease with increasing surface brightness. A similar correlation was reported for giant elliptical galaxies (Kormendy 1985) with much smaller dispersion. The largest source of dispersion is the dS0 galaxies which have regression coefficient, i.e., slope, of 1.67 ± 0.36 of which the error of the regression coefficient is about two times larger than those of other sub-types. This makes the correlation strength (cc=0.37) weaker than other sub-types. Among the five sub-types, dSph galaxies have the smallest slope (1.04 ± 0.16) which is manifested by their shallow surface brightness gradient. The dSph and dE_{blue} galaxies are quite well segregated in the M_r vs $\log(R_e)$ and $\langle \mu_e \rangle$ vs M_r diagrams as well as $\langle \mu_e \rangle$ vs $\log(R_e)$ diagram.

As mentioned above, the Sérsic index n shows weak dependence on other structural parameters. As shown in the middle right panel of Figure 4, dE-like dwarfs show decreasing $\langle \mu_e \rangle$ with increasing $\log(n)$, which have the regression coefficient of -0.93 ± 0.21 with cc = -0.14, for the whole sample. In contrast, if we examine the correlation between $\langle \mu_e \rangle$ and $\log(n)$ by considering the sub-types, there are large differences among sub-types. For instance, dSph galaxies show nearly no correlation between $\langle \mu_e \rangle$ and $\log(n)$, i.e., the regression coefficient of 0.53 ± 0.13 with cc = 0.29 and opposite trend for dS0 galaxies that have the regression coefficient of 0.65 ± 0.19 with cc = 0.29. The negative correlation of the dE-like galaxies is mainly due to the negative regression coefficients of dE, dE_{bc}, and dE_{blue} galaxies among which dE_{bc} galaxies have the strongest correlation with cc = -0.41. Because a large n indicates a steep luminosity gradient which results in high surface brightness in the inner part of a galaxy, the negative regression coefficients found for dE, dE_{bc}, and dE_{blue} galaxies seem to be natural. We present the results of correlation analysis among the structural parameters in the Appendix.

We examined the effect of nucleation on the correlations between structural parameters (M_r , n , $\langle \mu_e \rangle$, R_e) for dS0, dE, and dSph galaxies and found that there is no significant difference in most correlations. Figure 5 (dE galaxies) and Figure 6 (dS0 and dSph galaxies) show correlations between structural parameters which seem to be of interest. As shown in the upper left panel of Figure 5, there is a weak correlation between $\langle \mu_e \rangle$ and $\log(n)$ in nucleated dEs (denoted by red filled circles) with cc = -0.38, while there is no correlation in non-nucleated dEs (denoted by black crosses) with cc = 0.01. In contrast, there is no considerable difference in the correlation between $\langle \mu_e \rangle$ and $\log(R_e)$ presented in the upper right panel of Figure 5. As can be seen in these figures, there is no non-nucleated dEs that have surface brightness brighter than $\langle \mu_e \rangle \approx 22$. Most high surface brightness dEs are due to strong nucleation. While the relation between M_r and $\log(R_e)$ shows strongest correlation among the correlations between struc-

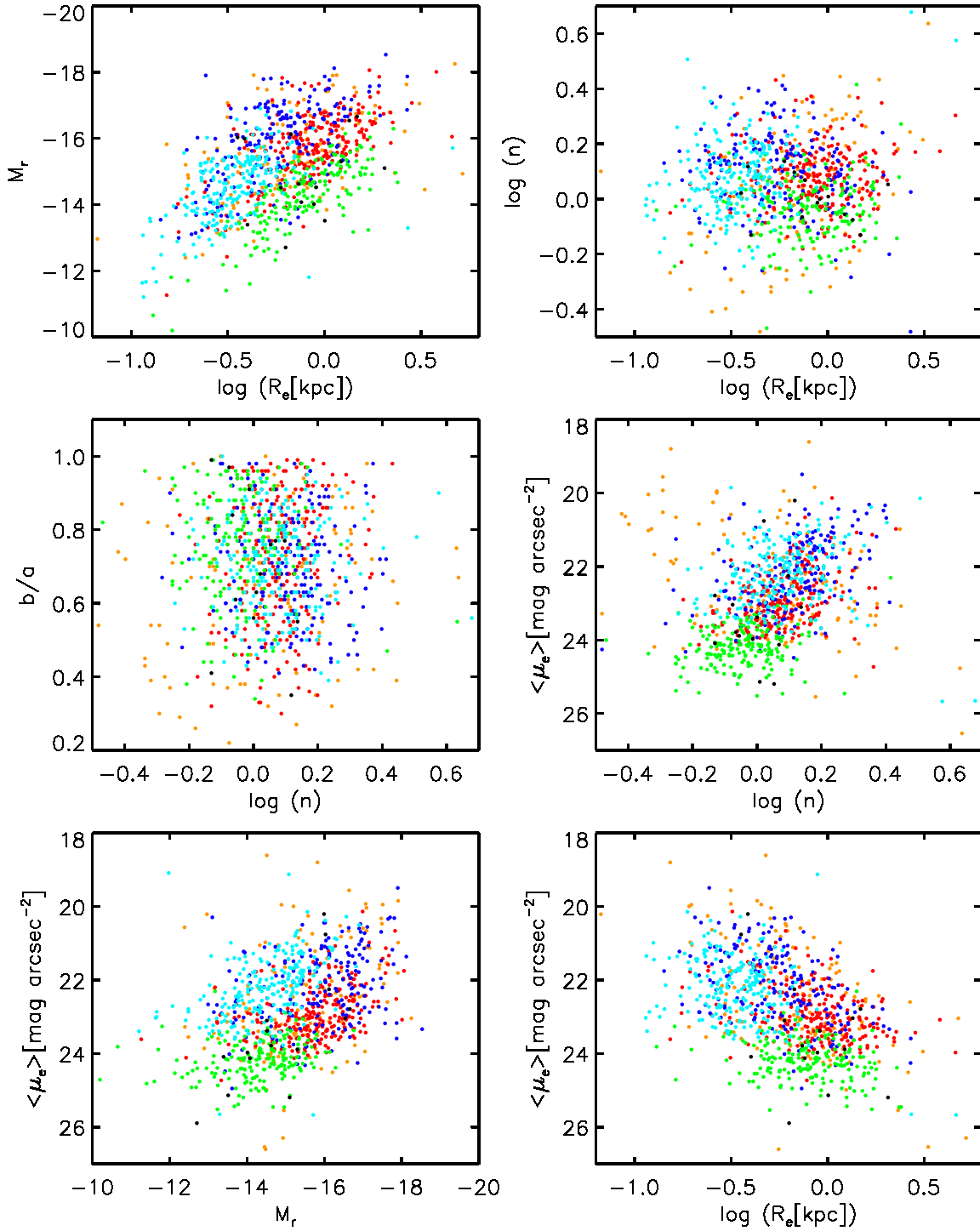


Figure 4. Correlations between GALFIT parameters of dE-like galaxies. (Top left) $\log(R_e)$ vs M_r , (top right) $\log(R_e)$ vs $\log(n)$, (Middle left) $\log(n)$ vs b/a , (middle right) $\log(n)$ vs $\langle \mu_e \rangle$, (bottom left) M_r vs $\langle \mu_e \rangle$, (bottom right) $\log(R_e)$ vs $\langle \mu_e \rangle$. Colour codes are orange(dS0), red(dE), blue(dE_{bc}), green(dSph), and cyan(dE_{blue}).

tural parameters of dE galaxies, there is no appreciable difference between nucleated dEs and non-nucleated dEs. They show regression coefficients of -3.02 ± 0.25 and -3.25 ± 0.46 , respectively. However, there is some difference in the luminosity as shown in the lower left panel of Figure 5. There are a lot of bright nucleated dEs compared with the mean relation between M_r and $\log(R_e)$ of non-nucleated dEs. The difference in the luminosity distribution

between nucleated dEs and non-nucleated dEs are more easily seen in the $\log(n)$ vs $\log(R_e)$ diagram presented in the lower right panel of Figure 5 which shows no correlation for both nucleated and non-nucleated dEs.

Figure 6 shows the correlations between structural parameters for dS0 and dSph galaxies. For the correlation between $\langle \mu_e \rangle$ and $\log(n)$, shown in the top panels, the effect of nucleation is somewhat

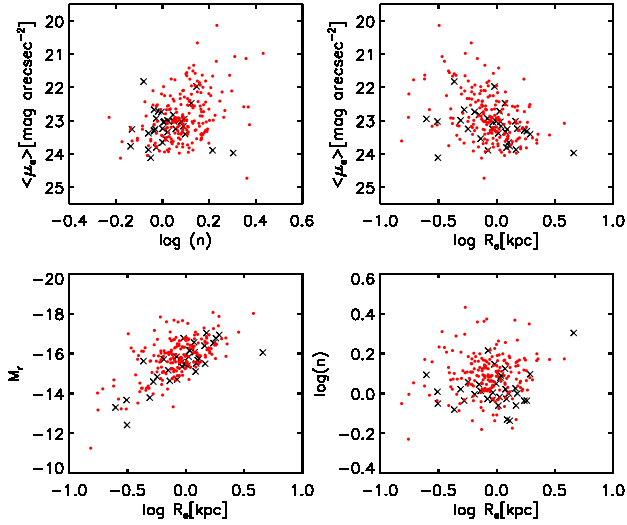


Figure 5. Correlation of structural parameters of dE galaxies distinguished by nucleation. The galaxies with nucleation are plotted as red filled circles and those without nucleation are designated by black crosses.

pronounced in dSph galaxies but negligible in dS0 galaxies. The correlations show opposite trend in nucleated and non-nucleated dSphs although they show negligible ($cc = 0.11$) and weak ($cc = -0.33$) correlation respectively for nucleated and non-nucleated dSphs. As shown in the middle panels, contrary to the case for dE galaxies, there is a significant difference in the correlations between M_r and $\log(R_e)$ for nucleated and non-nucleated dSphs because the regression coefficient of nucleated dSphs is -2.7 ± 0.26 with confidence interval of $(-3.96, -1.24)$ while that of non-nucleated dSphs is -5.03 ± 0.38 with the confidence intervals of $(-6.97, -4.53)$. Since they have $cc = -0.65$ for nucleated dSphs and $cc = -0.94$ for non-nucleated dSphs, The dS0 galaxies show a similarly significant difference in the correlation between M_r and $\log(R_e)$. Their regression coefficients are -3.45 ± 0.38 with confidence interval of $(-5.12, -2.26)$ for nucleated dS0s and -1.39 ± 0.38 with confidence interval of $(-2.21, -0.43)$ for non-nucleated dS0s, respectively. But, there are differences in the regression coefficients between dSphs and dS0s. Steeper slope is found in the non-nucleated dSphs while steeper slope is found in the nucleated dS0s. For the correlations between $\log(n)$ and $\log(R_e)$, dSph galaxies show no difference between nucleated and non-nucleated dSphs whereas dS0 galaxies show a clear difference because the slopes are opposite. However, this difference is not statistically significant since the slope of nucleated dS0s is within the confidence interval of the slope of non-nucleated dS0s.

The absence of a significant difference in most correlations for structural parameters between the nucleated and non-nucleated dwarfs is due to the small size of the nuclear region that is difficult to affect the global structure of galaxies. Moreover, we derived the structural parameters using two component models for these galaxies, one for the nucleus and the other for the main body of galaxies. Hence, the structural parameters are not much affected by the presence of the nucleus.

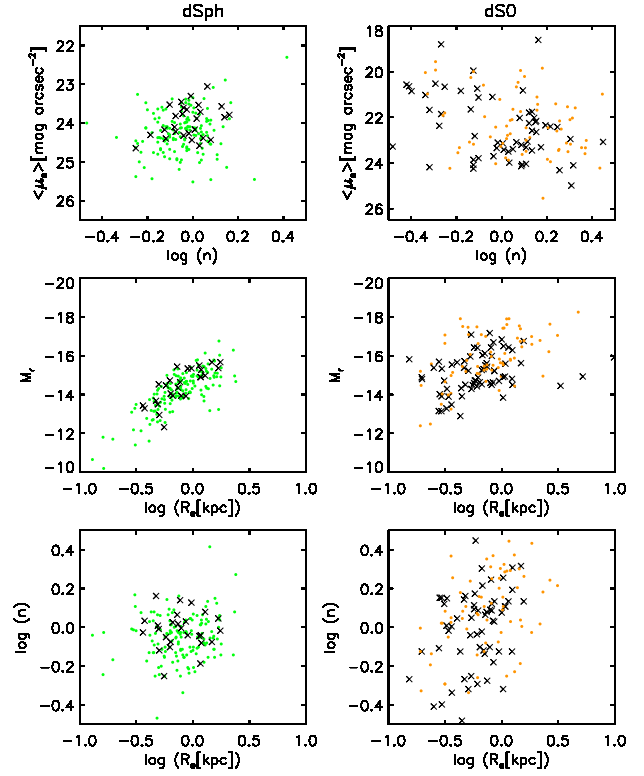


Figure 6. Correlation between structural parameters of dS0 and dSph galaxies distinguished by nucleation, dSph in the left column and dS0 in the right column. The galaxies with nucleation are plotted as coloured filled circles and those without nucleation are designated by black crosses.

3.4 Environmental Dependence of Structural Parameters

We use the local galaxy density as a measure of environment. We derive the local galaxy density from the n th nearest neighbour method with $n = 5$,

$$\Sigma = \frac{n}{4\pi r_{p,n}^2}$$

where $r_{p,n}$ is the projected distance from the target galaxy to the n th nearest neighbour galaxy. Criteria of selecting neighbour galaxies are the same as those adopted by Ann (2017). That is, we use the two parameters, M_r^* and ΔV^* , to constrain the neighbour galaxies. The former parameter (limiting magnitude) is set to $M_r^* = -15.2$ and the latter (linking velocity) is set to $\Delta V^* = 1000 \text{ km s}^{-1}$. We normalize the local galaxy density (Σ) by the mean local galaxy density ($\bar{\Sigma}$) derived for the galaxies in the local universe ($z \lesssim 0.01$) using SDSS DR7.

Figure 7 shows the distribution of the local galaxy density of the five sub-types of dE-like galaxies. There is little difference among the three types of dS0, dE, and dSph which are located in the high density regions. The local galaxy densities of dE_{bc} and dE_{blue} galaxies are much different from those of dS0, dE and dSph galaxies with a larger difference in dE_{blue} galaxies. The distribution of the local galaxy density of dE_{bc} galaxies is similar to that of dE_{blue} galaxies but it shows more fraction in high density regions than dE_{blue}. The low density tails of the three types (dS0, dE and dSph) are partly due to the galaxies in the survey boundary. However, some of them are thought to be genuinely extremely isolated galaxies.

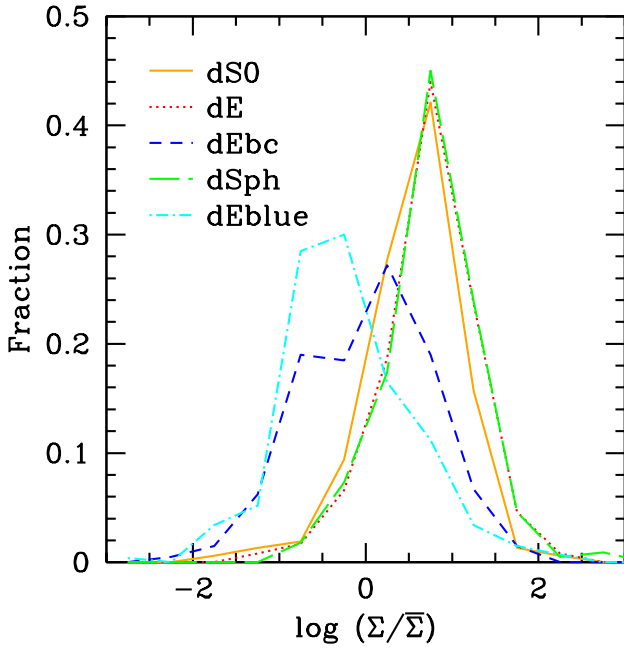


Figure 7. Local galaxy density distributions ($\Sigma/\bar{\Sigma}$) of dwarf elliptical-like galaxies.

The environmental dependence of the structural parameters (n , R_e , and $\langle \mu_e \rangle$) of dE-like galaxies is explored using scatter diagrams as shown in Figure 8. There is not much difference in the local galaxy densities of dS0, dE, and dSph galaxies which are somewhat different from those of dE_{bc} and dE_{blue}. As shown in Figure 8, the local galaxy density of each sub-type of dE-like galaxies spreads largely with the mean local galaxy densities of 0.56 ± 0.55 , 0.74 ± 0.57 , 0.03 ± 0.73 , 0.75 ± 0.53 , and -0.22 ± 0.73 , for dS0, dE, dE_{bc}, dSph, and dE_{blue} galaxies, respectively. Among the five sub-types, on average, dE and dSph galaxies are located in the highest density regions while dE_{blue} galaxies are located in the lowest density regions. The non-negligible fraction of dE galaxies in the low density regions ($\log \Sigma/\bar{\Sigma} < -1$) is quite puzzling because dE galaxies are mostly observed in high density regions. However, some of them are not genuinely isolated galaxies but are located in the survey boundary. There are only a few dEs that are located in the low density regions with $\log \Sigma/\bar{\Sigma} < -1$. The local galaxy density of dE_{bc} galaxies overlaps with that of dE_{blue} in the low-density regions and those of dS0, dE, and dSph galaxies in the high-density regions. The low-density environment of dE_{blue} galaxies, similar to that of dwarf irregular (dI) galaxies reported in ANN15, along with their blue colours imply that they are dI galaxies with round shape. As a whole, there is no dependence of R_e on the local galaxy density and a weak dependence of $\log(n)$ and $\langle \mu_e \rangle$ on $\log(\Sigma/\bar{\Sigma})$. That is, Sérsic index (n) decreases with increasing local galaxy density, and $\langle \mu_e \rangle$ increases, i.e., becoming low surface brightness, with increasing local galaxy density.

3.5 Spiral features

The most striking features observed in a large number of dE-like galaxies are the underlying spiral structures which are thought to be closely related to their origin. We investigate the residual images obtained by subtracting the GALFIT model images from the observed ones to see the underlying structures. Examples of residual images

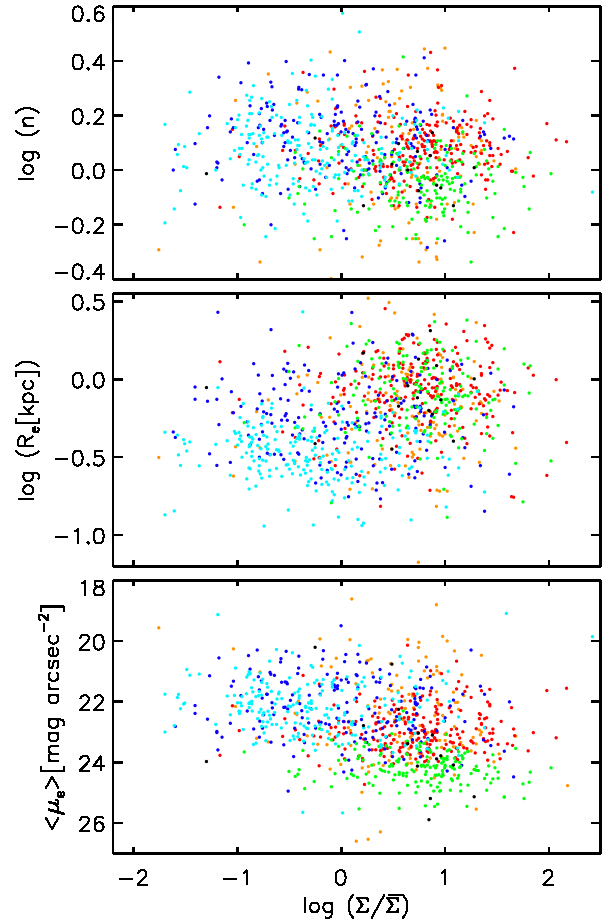


Figure 8. Local galaxy density ($\Sigma/\bar{\Sigma}$) versus three parameters n , R_e , and $\langle \mu_e \rangle$. Colour codes for sub-types are the same as Figure 3. (top) Sérsic index n , (middle) effective radius R_e , (bottom) mean surface brightness within $R_e < \mu_e$.

are given in Figure 9 where we can see features such as spiral arm remnants, bars, and rings. We refer them as disk features below. We summarize the fractions of five sub-types of dE-like galaxies that show disk features in Table 4 where the subscripts ' n ' and ' un ' denote the presence and absence of nucleation, respectively.

As shown in Table 4, about 17% of our sample of dE-like galaxies shows disk features in the residual images. However, the disk features we found are mainly observed in dS0 and dE galaxies, and the residual features of dE_{bc} and dE_{blue} galaxies are thought to be not spiral structures but irregular star forming regions. They are sometimes double or multiple core-like structures of enhanced star formation (see Figure 9). Therefore, if we consider spiral features in dS0, dE, and dSph galaxies only, it is increased to $\sim 20\%$ of these galaxies. This fraction is much larger than the results of Lisker et al. (2006) who reported 10% in the Virgo cluster, and a little smaller than $\sim 20 - 25\%$ fraction found in early-type dwarf galaxies in the Virgo and the Coma clusters (Aguerri 2016).

The highest frequency of spiral features ($\sim 34\%$) appears in dE galaxies. The dE with nucleation (dE_n) have spiral features in 38%. The difference in the fraction of spiral features between galaxies with and without nucleation is also pronounced in dE galaxies, 14% in dE_{un} and 38% in dE_n. However, the most interest finding

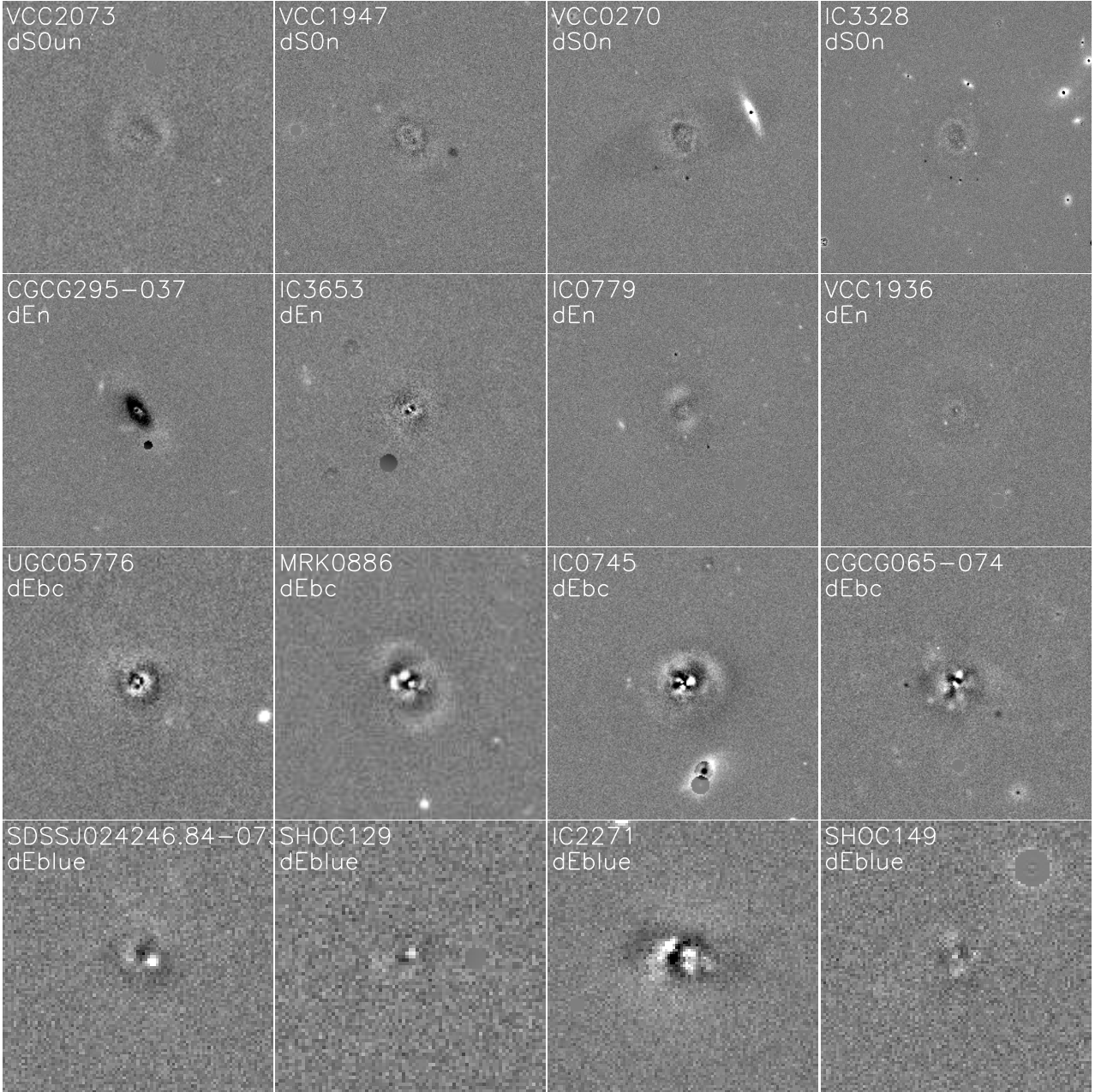


Figure 9. Sample of residual images of dwarf elliptical-like galaxies. (1st row) dS0 galaxies, (2nd row) dE galaxies, (3rd row) dE_{bc} galaxies, (4th row) dE_{blue} galaxies.

Table 4. The fraction of disk features of dE-like galaxies.

<i>type</i>	dS0	dS0 _{un}	dS0 _n	dE	dE _{un}	dE _n	dSph	dSph _{un}	dSph _n	dE _{bc}	dE _{blue}
fraction	0.25	0.19	0.32	0.34	0.14	0.38	0.00	0.00	0.01	0.16	0.09

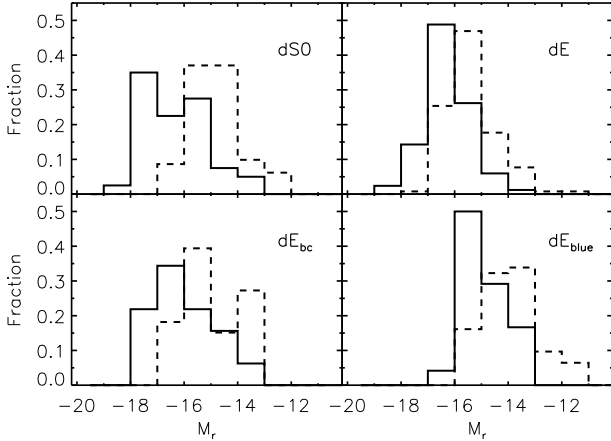


Figure 10. Frequency distribution of dE-like galaxies with and without disk features as a function of M_r . Galaxies showing disk features are plotted by solid lines and those showing no disk features are plotted by dashed lines. (upper left) dS0 galaxies, (upper right) dE galaxies, (bottom left) dE_{bc} galaxies, (bottom right) dE_{blue} galaxies

is the absence of disk features in dSph galaxies. If we apply a single component model to the luminosity distribution of dSph galaxies that have nucleation, some dSph galaxies show small features in residual images, but there is no disk features seen in the residual images obtained from the two component models of which one assumes a nuclear component.

Figure 10 shows the fractional frequency distributions of dE-like galaxies as a function of M_r , divided into galaxies with and without disk features. The galaxies with disk features are represented by solid lines and those without disk features are plotted by dashed lines. We except dSph galaxies because they do not show disk features. For most dE-like galaxies, disk features are more likely to be found in bright galaxies. This trend is most pronounced in dS0 galaxies of which disk features are mostly spiral arm remnants. There are only a small fraction of dS0 galaxies brighter than $M_r = -16$ that do not have disk features. Similar trend is found for dE and dE_{bc} galaxies that are brighter than $M_r = -17$. In dE_{blue} galaxies, the frequency distribution of disk features appears to be symmetrical in the sense that more galaxies with disk features at the bright part and more galaxies without disk features at the faint part.

Figure 11 shows the frequency distributions of Sérsic index in dE-like galaxies. We represent the galaxies with disk features by solid lines and those without disk features by dashed lines. In general, there is no significant difference between the galaxies with disk features and those without disk features. However, there is a weak tendency of a larger n for galaxies with disk features in dS0 and dE galaxies.

3.6 Environmental Dependence of Spiral Feature

The environmental dependence of the frequency distributions of disk features in dE-like galaxies is examined in Figure 12. As can be seen in Figure 12, there is no significant difference in the frequency distributions of the fraction of galaxies with disk features and those without disk features except for dE_{blue} galaxies which are likely to be located in the under-dense regions. However, there is some difference in the distribution of the local galaxy density for galaxies

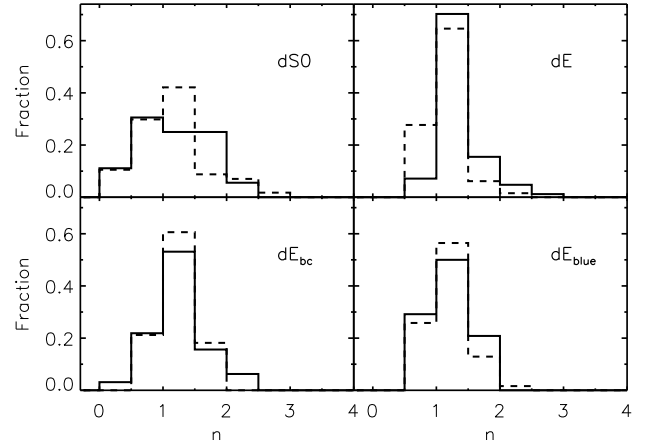


Figure 11. Frequency distribution of dE-like galaxies with and without disk features as a function of Sérsic index, n . Galaxies showing disk features are plotted by solid lines and those showing no disk features are plotted by dashed lines. (upper left) dS0 galaxies, (upper right) dE galaxies, (bottom left) dE_{bc} galaxies, (bottom right) dE_{blue} galaxies

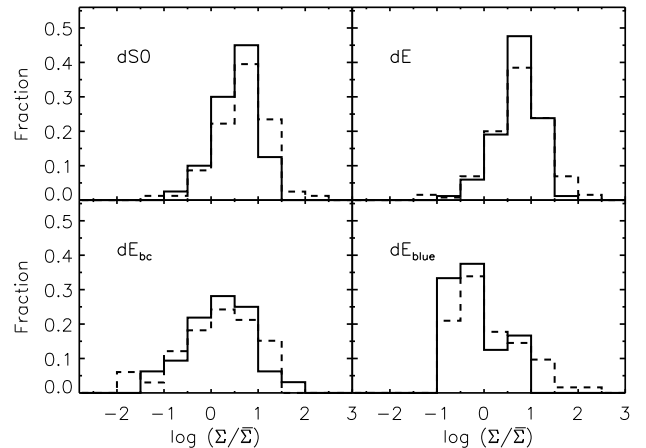


Figure 12. Frequency distribution of dE-like galaxies with and without disk features as a function of the local background density. Galaxies showing disk features are plotted by solid lines and those showing no disk features are plotted by dashed lines. (upper left) dS0 galaxies, (upper right) dE galaxies, (bottom left) dE_{bc} galaxies, (bottom right) dE_{blue} galaxies

with and without disk features. The dS0 and dE galaxies without disk features are more likely to be found in the high density regions. In particular, there is no dS0 galaxies with disk features in the local galaxy density higher than $\log(\Sigma/\bar{\Sigma}) \sim 1.5$. The dE galaxies show environmental dependence similar to dS0 galaxies but a negligible fraction of dE galaxies with disk features shows background density higher than $\log(\Sigma/\bar{\Sigma}) \sim 1.5$.

Among the dE-like galaxies, dE_{bc} galaxies show the broadest distribution of the local galaxy density but no significant difference between galaxies with disk features and those without disk features. Another feature worth to be noted is that a significant fraction of dE_{bc} galaxies are located in the low density regions with $\log(\Sigma/\bar{\Sigma}) < -1$. For dE_{blue} galaxies, they are prevalent at under-dense regions, regardless of the presence/absence of disk features. On the

contrary, at high density regions of $\log(\Sigma/\bar{\Sigma}) > 1$, dE_{blue} galaxies with no disk features are much more frequent than dE_{blue} with disk features. It seems to be related to the properties of the disk features in dE_{blue} galaxies. While the disk features in dS0 and dE galaxies are thought to be spiral arms, bars, and rings, which are leftover material after transformation from the late type disk galaxies to dS0 and dE galaxies, those observed in dE_{blue} galaxies are sites of ongoing active star formation. Since star formation is more active in the under-dense regions at the present time, dE_{blue} galaxies with disk features are more likely to be found in the under-dense regions as shown in the bottom right panel of Figure 12.

4 DISCUSSION

The terminology of dE-like galaxies used in the present study includes five sub-types of dwarf galaxies; dS0, dE, dSph, dE_{bc} , and dE_{blue} . Among them, the first three sub-types are frequently found in the literature to represent the early-type dwarf galaxies, whereas the others are new ones introduced by ANN15 to represent blue-cored dwarf elliptical galaxy (dE_{bc}) and globally blue dwarf galaxy with round shape (dE_{blue}). Ann (2017) considered dE_{bc} galaxies as early-type dwarfs and dE_{blue} as late-type dwarfs because of their active star formation like dwarf irregular (dI) galaxies. Actually, there is no difference between dE_{blue} and dI except for the roundness. They are very similar to HII region-like BCDs with somewhat reduced star formation. The sub-types of dE-like galaxies are reported in some previous studies (Lisker et al. 2007; Karachentsev et al. 2013) but with different symbols. In particular, the classification system of dwarf galaxies by Karachentsev et al. (2013) includes all the sub-types of ANN15 if we consider dE_{blue} as HII region-like BCD. Thus, the sub-types of dE-like galaxies such as those employed in the present study is useful for a detailed analysis of the structural properties of dwarfs although there is no consensus on the symbols.

There is a considerable difference between the structural parameters of the five sub-types of dE-like galaxies. In particular the Sérsic index n of dSphs is clearly distinguished from that of dEs when we apply two-component model of which one component is the Sérsic function to represent the main body of a galaxy and the other component represent the nuclear light excess due to nucleation. The K-S test of the distribution of n for the two sub-types are statistically different with $p < 0.05$ for most cases. The difference in the Sérsic index between dSphs and dEs reflects the morphological difference of the two sub-types. The morphology of dSphs is characterized by the lower surface brightness and shallower gradient in the luminosity distribution than dEs. The presence of nucleation does little affect the Sérsic index n fitted to the main body of dSphs and dEs. In contrast, there is no significant difference in n between dSphs and dEs if we neglect the nuclear component. Thus, proper treatment of the nuclear component is critical for a better understanding of the structure of early-type dwarfs since most early-type dwarfs show nucleation.

The noticeable difference in some structural parameters among sub-types of dE-like galaxies also supports the usefulness of sub-types in the classification of dwarf galaxies. For example, there is a pronounced difference in the mean surface brightness within the effective radius, $\langle \mu_e \rangle$ between dSph galaxies and others. The dSph galaxies have $\langle \mu_e \rangle = 24.2 \pm 0.8$ while other types have $\langle \mu_e \rangle \lesssim 23.0$ with the highest one in dE_{blue} as $\langle \mu_e \rangle = 22.2$. The small Sérsic index of dSph galaxies is closely related to the low surface brightness and the shallow gradient in the surface brightness.

Although the distinction of dSph galaxies from dE galaxies has been made clearly for the galaxies in the LG, many previous studies (e.g., Kormendy 1985) did not distinguish dSph galaxies from dE galaxies. However, dSph galaxies have structural properties different from those of dE galaxies besides the photometric properties. They are supposed to be pressure supported (Walker et al. 2009; Salucci et al. 2012) while dE galaxies are likely to be rotation supported (Pedraz et al. 2002; Simien & Prugniel 2002; Geha et al. 2003; van Zee et al. 2004; de Rijcke et al. 2005; Chilingarian 2009; Geha et al. 2010; Toloba et al. 2015; Penny et al. 2016). They are dark matter dominated galaxies with $M/L > 100$ (Gallagher & Wyse 1994; Mateo 1994; Pryor 1994, 1996; Gerhard 1994; Olszewski 1998; Battaglia et al. 2013; Simon & Geha 2021).

The lack of disk features in dSph galaxies, which is a unique property of dSph galaxies, provides a further observational evidence which make them different from dE galaxies. The deficit of disk features in faint early-type dwarf galaxies of the Virgo cluster was noticed by Lisker et al. (2006) who found that $> 50\%$ of early-type dwarfs at bright end have disk features while only a few percent of them have disk features at $m_B > 16$ which corresponds to $M_B \approx -15$. Since the majority of faint early-dwarf galaxies in the VCC are supposed to be dSph galaxies in ANN15, the lack of disk features in dSph galaxies is in a good agreement with Lisker et al. (2006).

Any scenarios for the origin of dSph galaxies are required to explain the aforementioned properties of dSph galaxies. In a broad category, there are two scenarios for the origin of dSph galaxies, of course dE-like galaxies in general. One is that they are primordial objects, i.e., they are the descendants of building blocks of the early universe. The other is that they are transformed objects from the late-type galaxies by the environmental effects (Lisker et al. 2007; Janz et al. 2014) such as ram pressure stripping (Gunn & Gott 1972) and galaxy harassment (Moore et al. 1998, 1999). While ram pressure stripping of the cold gas in the late-type galaxies leads to shutdown of star formation, galaxy harassment thickens the disk of a galaxy by tidal heating (Toth & Ostriker 1992) or tidal stripping. The small mass of dSph galaxies facilitates gas removal in these galaxies whether they are primordial objects or transformed ones. Since the mean stellar age of dSph galaxies which are originated from the primordial objects is thought to be much older than that of the dSph galaxies transformed from the late-type galaxies falling into cluster environment, analysis of stellar age is required to clarify their origin. We will present a detailed analysis of the SDSS spectra of the dE-like galaxies in the forthcoming papers.

The majority of early-type dE-like galaxies (dS0, dE, dSphs and dE_{bc}) are supposed to be transformed from late-type galaxies because most of the dE-like galaxies are located in group and cluster environment where environmental effects such as ram pressure stripping and galaxy harassment are expected to be operating. On the other hand, the primordial origin of the dE-like galaxies is also plausible because at least $\sim 5\%$ of them are isolated galaxies which do not suffer environmental effects to transform their morphology. Ann (2017) also showed that some dE and dSph galaxies which are satellites of isolated satellite systems are likely to be primordial objects because they are located in the outer part of the satellite systems where environmental effect is not effective. Thus, as noted by Lisker (2009), multiple origins of dE-like galaxies are very likely.

5 SUMMARY AND CONCLUSIONS

We examined the luminosity distributions and spiral features of the five sub-types of dE-like galaxies in the local universe ($z \lesssim 0.01$)

by applying GALFIT to the r -band SDSS images. We derived structural parameters such as the effective radius (R_e), the mean surface brightness within R_e ($\langle \mu_e \rangle$), axial ratio (b/a) along with the Sérsic index (n). The structural parameters of the dE-like galaxies overlap a lot among sub-types but the most likely structural parameters of each sub-type could be distinguished from others. In particular, $\langle \mu_e \rangle$ seems to be effective to distinguish dSph galaxies from other sub-types.

The distribution of the Sérsic index n of dE-like galaxies is much different from pure disk galaxies as well as elliptical galaxies. More than $\sim 90\%$ of dE-like galaxies have the Sérsic index between 0.5 and 2.0 except for the dE_{bc} galaxies of which $\sim 36\%$ of them have the Sérsic index larger than $n=2$. However, the detailed distribution of n depends on the sub-types. The dS0, dE, and dE_{blue} have the largest fractions at $n=1.0 \sim 1.5$ while dSph peaks at $n=0.5 \sim 1.0$ and dE_{bc} peaks at $n=1.5 \sim 2.0$. It is crucial to add a nuclear component to fit the luminosity distribution of dE-like galaxies because most dE-like galaxies show nucleation which leads to a larger n if we apply a single-component model to fit the observed luminosity distribution. The nuclear component is approximated by either King profile or Nuker profile. The K-S test for the distribution of the Sérsic index between sub-types shows that they are statistically different populations. The distinction between sub-types, in particular between dSph and dE, may cast some insight into their origins.

There are clear correlations between structural parameters, which depend on the sub-types. For example, the Pearson correlation coefficient (cc) for the relation between $\langle \mu_e \rangle$ and $\log(R_e)$ is 0.46. The structural parameters also correlate with the galaxy luminosity in the sense that bright galaxies have larger R_e and higher $\langle \mu_e \rangle$ than faint galaxies. The relation between the luminosity (M_r) and the mean surface brightness ($\langle \mu_e \rangle$) of the dE-like galaxies shows the same trend with the relation between the luminosity and the central surface brightness of early-type dwarf galaxies, that is the surface brightness of early-type dwarf galaxies, Sph in Kormendy's terminology, increases, i.e., becoming brighter, with increasing luminosity. This trend is opposite to the trend observed in the early-type giant galaxies (Kormendy 1985).

A significant fraction of dE-like galaxies show disk features such as spiral arm, bar, lens, and ring structures but it depends on sub-types. The two sub-types, dS0, and dE, have disk features in $\sim 30\%$ of them, whereas there is virtually no dSph galaxies that have disk features. The residual images of dE_{bc} and dE_{blue} galaxies show somewhat different features from those of dE and dS0. Especially, dE_{blue} galaxies show the star forming regions of irregular shapes rather than the spiral features. The dE_{bc} galaxies show mixed features. It is apparent that spiral arms are more frequent in the bright dS0 and dE galaxies but there is no correlation with the Sérsic index. The disk features are more likely to be found in the low density regions than the high density regions, however, the dependence is very weak. The presence and absence of nucleation do not affect the disk features of dS0 galaxies but more frequent disk features in the nucleated dE galaxies. On the other hand, disk features depend strongly on the galaxy luminosity. The fraction of disk features is largest at the bright end of dE-like galaxies. The absence of disk features in dSph galaxies is in a good agreement with the luminosity dependence of disk features.

It seems likely that the majority of the three sub-types of dE-like galaxies (dS0, dE, and dE_{bc}) are transformed from the late-type galaxies in groups and clusters but there is other route for the formation of these galaxies.

ACKNOWLEDGMENTS

This work was supported partially by the NRF Research grant 2015R1D1A1A09057394.

DATA AVAILABILITY

The original data underlying this article are available in SDSS DR7. And additional data are available upon request.

REFERENCES

- Abazajian K. N., et al., 2009, *ApJS*, **182**, 543
- Aguerre J. A. L., 2016, *A&A*, **587**, A111
- Ann H. B., 2017, *JKAS*, **50**, 111
- Ann H. B., Lee H.-R., 2013, *JKAS*, **46**, 141
- Ann H. B., Seo M., Ha D. K., 2015, *ApJS*, **217**, 27
- Barazza F. D., Binggeli B., Jerjen H., 2002, *A&A*, **391**, 823
- Battaglia G., Helmi A., Breddels M., 2013, *New Astron. Rev.*, **57**, 52
- Binggeli B., Jerjen H., 1998, *A&A*, **333**, 17
- Binggeli B., Sandage A., Tammann G. A., 1985, *AJ*, **90**, 1681
- Blanton M., 2003, Comparing the ACS Ultra Deep Field to Low Redshift Galaxy Observations, HST Proposal
- Boselli A., Gavazzi G., 2014, *A&ARv*, **22**, 74
- Chilingarian I. V., 2009, *MNRAS*, **394**, 1229
- Choi Y.-Y., Han D.-H., Kim S. S., 2010, *JKAS*, **43**, 191
- De Rijcke S., Dejonghe H., Zeilinger W. W., Hau G. K. T., 2003, *A&A*, **400**, 119
- Elmegreen D. M., Elmegreen B. G., 1982, *MNRAS*, **201**, 1021
- Elson R. A. W., 1999, in *Globular Clusters*, pp 209–248
- Ferguson H. C., Binggeli B., 1994, *A&ARv*, **6**, 67
- Gallagher John S. I., Wyse R. F. G., 1994, *PASP*, **106**, 1225
- Geha M., Guhathakurta P., van der Marel R. P., 2002, *AJ*, **124**, 3073
- Geha M., Guhathakurta P., van der Marel R. P., 2003, *AJ*, **126**, 1794
- Geha M., van der Marel R. P., Guhathakurta P., Gilbert K. M., Kalirai J., Kirby E. N., 2010, *ApJ*, **711**, 361
- Gerhard O. E., 1994, in *European Southern Observatory Conference and Workshop Proceedings*, p. 335
- Gilmore G., Wilkinson M. I., Wyse R. F. G., Kleya J. T., Koch A., Evans N. W., Grebel E. K., 2007, *ApJ*, **663**, 948
- Graham A. W., Jerjen H., Guzmán R., 2003, *AJ*, **126**, 1787
- Grant N. I., Kuipers J. A., Philipps S., 2005, *MNRAS*, **363**, 1019
- Grebel E. K., 1997, *Reviews in Modern Astronomy*, **10**, 29
- Gunn J. E., Gott J. Richard I., 1972, *ApJ*, **176**, 1
- Janz J., et al., 2014, *ApJ*, **786**, 105
- Jerjen H., Kalnajs A., Binggeli B., 2000, *A&A*, **358**, 845
- Karachentsev I. D., Makarov D. I., Koisina E. I., 2013, *AJ*, **145**, 101
- Kim K. H., Lee K.-H., Ann H. B., 2006, *JKAS*, **39**, 57
- Kim S., et al., 2014, *ApJS*, **215**, 22
- Koch A., Kleya J. T., Wilkinson M. I., Grebel E. K., Gilmore G. F., Evans N. W., Wyse R. F. G., Harbeck D. R., 2007, *AJ*, **134**, 566
- Kormendy J., 1985, *ApJ*, **295**, 73
- Kormendy J., Bender R., 2012, *ApJS*, **198**, 2
- Lauer T. R., et al., 1995, *AJ*, **110**, 2622
- Lisker T., 2009, *AN*, **330**, 1043
- Lisker T., Grebel E. K., Binggeli B., 2006, *AJ*, **132**, 497
- Lisker T., Grebel E. K., Binggeli B., Glatt K., 2007, *ApJ*, **660**, 1186
- Makarov D., Karachentsev I., 2011, *MNRAS*, **412**, 2498
- Mateo M., 1994, in *European Southern Observatory Conference and Workshop Proceedings*, p. 309
- Mateo M. L., 1998, *ARA&A*, **36**, 435
- Mayer L., Governato F., Colpi M., Moore B., Quinn T., Wadsley J., Stadel J., Lake G., 2001, *ApJ*, **559**, 754
- Moore B., Lake G., Katz N., 1998, *ApJ*, **495**, 139
- Moore B., Lake G., Quinn T., Stadel J., 1999, *MNRAS*, **304**, 465
- Mould J. R., et al., 2000, *ApJ*, **529**, 786

- Olszewski E. W., 1998, in Zaritsky D., ed., *Astronomical Society of the Pacific Conference Series Vol. 136, Galactic Halos*. p. 70
- Park C., Choi Y.-Y., 2005, [ApJL](#), **635**, L29
- Park C., Choi Y.-Y., Vogeley M. S., Gott J. Richard I., Blanton M. R., SDSS Collaboration 2007, [ApJ](#), **658**, 898
- Pedraz S., Gorgas J., Cardiel N., Sánchez-Blázquez P., Guzmán R., 2002, [MNRAS](#), **332**, L59
- Peng C. Y., Ho L. C., Impey C. D., Rix H.-W., 2002, [AJ](#), **124**, 266
- Peng Y.-j., et al., 2010, [ApJ](#), **721**, 193
- Penny S. J., et al., 2016, [MNRAS](#), **462**, 3955
- Pryor C., 1994, in *European Southern Observatory Conference and Workshop Proceedings*. p. 323
- Pryor C., 1996, in Morrison H. L., Sarajedini A., eds, *Astronomical Society of the Pacific Conference Series Vol. 92, Formation of the Galactic Halo...Inside and Out*. p. 424
- Ryden B. S., Terndrup D. M., Pogge R. W., Lauer T. R., 1999, [ApJ](#), **517**, 650
- Salucci P., Wilkinson M. I., Walker M. G., Gilmore G. F., Grebel E. K., Koch A., Frigerio Martins C., Wyse R. F. G., 2012, [MNRAS](#), **420**, 2034
- Sandage A., Binggeli B., 1984, [AJ](#), **89**, 919
- Shen S., Mo H. J., White S. D. M., Blanton M. R., Kauffmann G., Voges W., Brinkmann J., Csabai I., 2003, [MNRAS](#), **343**, 978
- Simien F., Prugniel P., 2002, [A&A](#), **384**, 371
- Simon J. D., Geha M., 2021, [Physics Today](#), **74**, 30
- Stoughton C., et al., 2002, [AJ](#), **123**, 485
- Toloba E., et al., 2015, [ApJ](#), **799**, 172
- Toth G., Ostriker J. P., 1992, [ApJ](#), **389**, 5
- Walker M. G., Mateo M., Olszewski E. W., Peñarrubia J., Evans N. W., Gilmore G., 2009, [ApJ](#), **704**, 1274
- York D. G., et al., 2000, [AJ](#), **120**, 1579
- de Rijcke S., Michielsen D., Dejonghe H., Zeilinger W. W., Hau G. K. T., 2005, [A&A](#), **438**, 491
- del Pino A., Aparicio A., Hidalgo S. L., Łokas E. L., 2017, [MNRAS](#), **465**, 3708
- van Zee L., Skillman E. D., Haynes M. P., 2004, [AJ](#), **128**, 121
- van den Bergh S., 1999, [A&ARv](#), **9**, 273

APPENDIX A: SOME EXTRA MATERIAL

Table A1 summarizes the correlation analysis applied to the data show in Figure 4. The columns give the following information. We applied linear least-squares fittings ($Y = a + bX$) and calculated the Pearson correlation coefficients and the confidence interval for the slope from bootstrap resampling.

This paper has been typeset from a \LaTeX file prepared by the author.

Table A1. The correlation analysis of the structural parameters.

Parameters	Galaxy type	a (intercept)	b (slop)	Standard deviation	Pearson coefficient	Confidence interval
M_r vs. $\log(R_e)$	dS0	-15.93±0.12	-2.74±0.29	1.20	-0.63	(-3.89,-1.65)
	dE	-15.96±0.06	-3.00±0.22	0.82	-0.67	(-3.66,-2.40)
	dE _{bc}	-16.56±0.10	-2.88±0.29	0.98	-0.59	(-3.45,-2.34)
	dSph	-14.52±0.07	-3.18±0.23	0.86	-0.71	(-4.53,-1.85)
	dE _{blue}	-15.92±0.13	-3.09±0.24	0.93	-0.65	(-4.25,-1.85)
< μ_e > vs. $\log(n)$	dS0	21.58±0.26	0.65±0.19	1.54	0.29	(0.33,1.05)
	dE	23.89±0.18	-0.79±0.14	0.67	-0.35	(-1.16,-0.40)
	dE _{bc}	23.63±0.26	-1.11±0.18	1.02	-0.41	(-1.44,-0.80)
	dSph	23.73±0.14	0.53±0.13	0.64	0.29	(-0.12,1.86)
	dE _{blue}	22.42±0.19	-0.20±0.14	1.12	-0.09	(-0.78,0.47)
< μ_e > vs. M_r	dS0	27.75±1.29	0.35±0.08	1.51	0.34	(0.15,0.48)
	dE	26.84±0.63	0.25±0.04	0.67	0.38	(0.12,0.35)
	dE _{bc}	26.07±1.04	0.25±0.07	1.08	0.27	(0.12,0.38)
	dSph	25.7±0.57	0.10±0.04	0.66	0.19	(0.01,0.16)
	dE _{blue}	25.55±0.86	0.23±0.06	1.09	0.25	(-0.09,0.45)
< μ_e > vs. $\log(R_e)$	dS0	22.67±0.14	1.67±0.36	1.49	0.37	(0.47,2.65)
	dE	22.99±0.05	1.06±0.18	0.67	0.36	(0.63,1.47)
	dE _{bc}	22.67±0.10	2.14±0.29	0.99	0.47	(1.59,2.65)
	dSph	24.34±0.05	1.04±0.16	0.60	0.43	(0.19,1.84)
	dE _{blue}	22.98±0.14	1.75±0.27	1.03	0.40	(1.20,2.45)